



Geometric phase of a two-level atom near a dielectric nanosphere out of thermal equilibriumEhsan Amooghorban ^{1,2,*}, Sareh Shahidani ³, and Somaye Mohamadi Abdhvand¹¹*Department of Physics, Faculty of Science, Shahrekord University P. O. Box 115, Shahrekord 8818634141, Iran*²*Nanotechnology Research Center, Shahrekord University, Shahrekord 8818634141, Iran*³*Department of Physics, Sharif University of Technology, Tehran 14588, Iran*

(Received 23 April 2024; revised 11 August 2024; accepted 29 August 2024; published 10 September 2024)

We study the geometric phase (GP) of a two-level atom coupled to an environment composed of free space and a dielectric nanosphere in thermal and out of thermal equilibrium. We analytically and numerically analyze the optical properties and loss of the dielectric medium, along with the nonequilibrium effects of the environment on the GP. In the weak coupling limit, we find that the correction to the GP depends on the partial local density of photonic states at the atom position, and an effective parameter that emerges out of the nonequilibrium configuration of the system. The GP exhibits a significant enhancement due to the excitation of evanescent surface waves at its resonance frequency. It is shown that the GP acquired by the atomic system out of thermal equilibrium is always bounded between the thermal-equilibrium counterparts. Furthermore, the temperature difference between the nanosphere and free space can play an important role in the GP only at moderate atomic distances from the nanosphere. Our results elegantly demonstrate properties of the GP near material media that can support phononic modes and pave the way for further research of GP as a resource for quantum computation.

DOI: [10.1103/PhysRevA.110.033710](https://doi.org/10.1103/PhysRevA.110.033710)**I. INTRODUCTION**

Pancharatnam [1] was first to introduce the concept of geometric phase (GP) to the classical optics, and then Berry [2] discovered this concept in quantum mechanics. He showed that a quantum system can acquire a GP upon adiabatic transport of its Hamiltonian around a closed path in parameter space or in the projective Hilbert space. It depends only on the geometry of the path that is taken and occur in a wide range of circumstances in both classical and quantum systems, such as Foucault's pendulum [3] and the Aharonov-Bohm effect [4]. Over the past decades, the original adiabatic GP has been generalized to different closed and open quantum systems undergoing nonadiabatic or noncyclic evolution [5–9]. Recently, the GP has shown great potential for applications in quantum computation, quantum sensing, and quantum information processing [10–16].

The presence of decoherence and dissipation due to interactions with the environment can modify the GP. In such cases, the GP can still provide valuable information about the system-environment interaction and its effects on the system's evolution. In the context of open quantum systems, different approaches have been applied to explore the modification of the GP caused by the external environment [17–24]. Understanding the influence of the environment on the GP is an important issue. It demonstrates the resilience of the GP to various types of noises, while also shedding light on how information about the environment is encoded in the GP. Many works have been conducted along these lines, considering different types of decoherence sources in both Markovian

and non-Markovian environments [25–34], the nonequilibrium environment [35], and strong coupling regime [36].

The two-level system, which is the focus of this study, and harmonic oscillator are the simplest and yet most significant examples for exploring GP in the context of open quantum system. Measuring the GP of these simple systems can be used as a tool to get information about the environment [33,34,37,38] and detect quantum effects like the Unruh effect [39] and quantum friction force [40]. In Ref. [37], GP encodes information about the number of particles in the surrounding quantized field. In Ref. [33], it is shown that GP of a dephasing two-level system contains phase information of the environment. In Refs. [39,41], it is shown that the two-level system can be used as a high-precision quantum thermometer, when its GP is affected by surrounding quantized field in thermal state.

The purpose of this paper is to study how GP of a two-level system is affected by decoherence and dissipation of the environment composed of free space and a dielectric nanosphere. Here, the dielectric medium with certain susceptibility and temperature modifies the quantum vacuum field. Depending on the relative distance between the atom and the dielectric medium as well as their geometrical and optical properties, this mechanism results in varying dissipation rate. Furthermore, when the atom is situated in a stationary configuration out of thermal equilibrium, where the medium temperature is maintained fixed and different from the surrounding free space, the density matrix of the atom evolves into a nonequilibrium steady state with an effective temperature [42,43]. Consequently, the GP of the atomic system can be expected to encode information about the geometrical and optical properties of the dielectric medium along with its temperature, and the nonequilibrium effects of the environment.

*Contact author: ehsan.amooghorban@sku.ac.ir

Recently, much attention has been paid to studying the nonequilibrium effects of the environment on dynamical evolution and decoherence of open quantum systems. The lack of thermal equilibrium may appear in transient and ultrafast processes in physical or biological systems, providing significant possibilities not available in the thermal equilibrium state, such as the suppression of the decoherence and the non-Markovian features of the quantum systems [44]. In this study, we compute the GP of the atomic system under nonunitary dynamics in both equilibrium and nonequilibrium configurations. The environmentally induced corrections to the GP can be decomposed in different contributions: medium correction induced by the modified quantum vacuum field due to the presence of the nanosphere and corrections induced by out of thermal equilibrium effects of the system.

The structure of this paper is organized as follows. In Sec. II, we introduce the model under investigation and obtain an exact master equation for the reduced atomic density operator to describe the dynamics of a two-level atom coupled to the quantized electromagnetic field in the presence of a nanosphere. We derive explicitly the atomic transition rates in terms of the partial local density of states and an effective parameter, which depend on material properties of the nanosphere, the atom position, and the orientation of the atom's dipole moment. In Sec. III, we compute the GP acquired by the atomic system in both equilibrium and nonequilibrium configurations. Section IV contains the numerical analysis of the medium- and nonequilibrium-induced corrections to the GP when the nanosphere is made of gallium arsenide, and compares them with those obtained when the atom is alone in free space. In the small-sphere limit, we derive expressions for the GP correction acquired by the atom in both short-distance and long-distance cases, and some experimental proposals for measuring the GP are discussed. Finally, in Sec. V, we make our final remarks and summary of the conclusions. Details on the derivation of the electromagnetic Green's tensor of the system found in Appendix A. The components of the Green's tensor as well as the partial local density of states in the small-sphere limit are derived in Appendix B.

II. MODEL

We consider a two-level atom with the transition frequency ω_0 in the vicinity of a dissipative-dispersive dielectric sphere with permittivity $\epsilon(\omega)$ and the radius a in a stationary configuration out of thermal equilibrium, as schematically shown in Fig. 1. The sphere and the surrounding vacuum are maintained at different constant temperatures, T_1 and T_0 , respectively. This can be done by connecting an external energy source at temperature T_1 to the sphere and embedding it in a thermal black-body radiation emitted by some walls far from both the sphere and the atom at temperature T_0 [45,46]. The distance from the atom to the center of the nanosphere is \mathbf{r}_a . The atom interacts with the sphere via the quantized electromagnetic field at the position of the atom. The quantization of the electromagnetic field in the presence of dissipative and dispersive dielectric media is accomplished in a second-quantization framework [47]. The framework is well known and has been carried out through the canonical [48–61] and

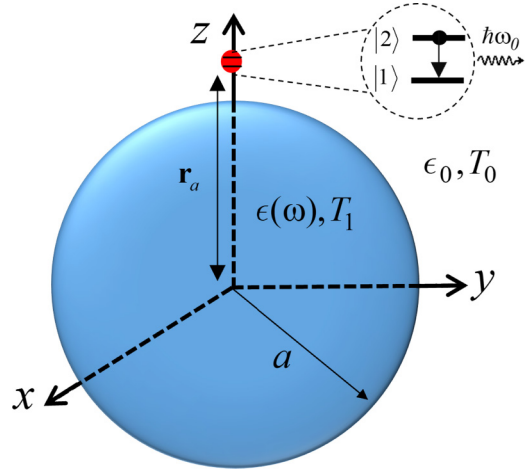


FIG. 1. A schematic of the system that is out of thermal equilibrium but in a stationary regime. It consists of a two-level atom located at the distance \mathbf{r}_a from the center of a dielectric sphere with permittivity function $\epsilon(\omega)$ and the radius a at temperature T_1 . The atom-nanosphere is embedded in a vacuum environment with free-space permittivity ϵ_0 at temperature T_0 .

phenomenological approaches [56–61]. We follow the rigorous canonical approach where the dielectric medium is modeled as a reservoir consisting of infinite harmonic oscillators. These harmonic oscillators, which characterized by a medium field, provide the polarizability and lossy characters of the medium. In this way, the dissipative medium enters directly into the quantization scheme, so that the complex frequency-dependent permeability of the medium is characterized through the macroscopic parameters of our model. Furthermore, the initial conditions of the medium field determines the explicit form of the current noise operator (more details can be found in Refs. [52,62,63]). Based on this quantization scheme, the Hamiltonian of the entire system is given by

$$H = H_a + H_f + H_{\text{int}}, \quad (1)$$

where

$$H_a = \hbar\omega_0 \sigma^+ \sigma^-, \quad (2a)$$

$$H_f = \int d^3\mathbf{r} \int_0^\infty d\omega \hbar\omega \mathbf{f}^\dagger(\mathbf{r}, \omega) \cdot \mathbf{f}(\mathbf{r}, \omega), \quad (2b)$$

$$H_{\text{int}} = -\mathbf{D} \cdot \mathbf{E}(\mathbf{r}_a, t) \quad (2c)$$

are, respectively, the usual Hamiltonian of the free atom, the Hamiltonian of the medium-assisted electromagnetic field, and the dipolar atom-field interaction Hamiltonian in the rotating wave approximation. Here, σ^- (σ^+) denotes the lowering (raising) operator of the atom, the annihilation and creation operators \mathbf{f} and \mathbf{f}^\dagger represent the collective excitations of the electromagnetic fields, and the medium and satisfy the canonical commutation relation $[f_i(\mathbf{r}, \omega), f_j^\dagger(\mathbf{r}', \omega')] = \delta_{ij} \delta(\mathbf{r} - \mathbf{r}') \delta(\omega - \omega')$, $\mathbf{E}(\mathbf{r}_a, t)$ is the electric field operator at the atom's position, and $\mathbf{D} = \mathbf{d}_{21}|2\rangle\langle 1| + \mathbf{d}_{12}^*|1\rangle\langle 2|$ is the electric dipole moment of the atomic system. Given that the vacuum (dielectric sphere) is in local thermal equilibrium at constant temperature T_0 (T_1), the correlation functions

between the elementary excitations of the system in a stationary configuration have the following form [64]:

$$\langle \mathbf{f}(\mathbf{r}, \omega) \mathbf{f}^\dagger(\mathbf{r}', \omega') \rangle = [1 + n(\omega, T_i)] \delta(\mathbf{r} - \mathbf{r}') \delta(\omega - \omega'), \quad (3a)$$

$$\langle \mathbf{f}^\dagger(\mathbf{r}, \omega) \mathbf{f}(\mathbf{r}', \omega') \rangle = n(\omega, T_i) \delta(\mathbf{r} - \mathbf{r}') \delta(\omega - \omega'), \quad (3b)$$

where $n(\omega, T_i) = 1/(\exp[\hbar\omega/k_B T_i] - 1)$.

A. Master equation

In this paper, we intend to compute the GP of the atomic system interacting with the medium-assisted electromagnetic field during its evolution at stationary but nonequilibrium condition. To explore a general description of the atom dynamics, we start from the von Neumann equation $\dot{\rho}_{\text{tot}}(t) = -\frac{i}{\hbar}[H_{\text{int}}^I(t), \rho_{\text{tot}}]$, where ρ_{tot} is the density operator of the combined close system and H_{int}^I is the interaction Hamiltonian (2c) in the interaction representation. Within the Born-Markov and rotating wave approximations, we trace out the photonic degrees of freedom and obtain the following master equation of the atom alone whose projections on the basis of the atomic subspace [65]

$$\dot{\rho}(t) = -\frac{i}{\hbar}[H_a + H_{LS}, \rho(t)] + \mathcal{D}[\rho(t)]. \quad (4)$$

The first term in the above equation describes the unitary evolution of the reduced density operator, and $\mathcal{D}[\rho(t)]$ is the Lindblad dissipator introducing dissipative effects such as relaxation or dephasing. Here, the Lamb-shift Hamiltonian

$$H_{LS} = \hbar(S(-\omega_0)|1\rangle\langle 1| + S(\omega_0)|2\rangle\langle 2|), \quad (5)$$

induces a shift of the atomic energy levels with a renormalized energy level spacing $\Omega(\omega_0) = \omega_0 + S(\omega_0) - S(-\omega_0)$, wherein $S(\omega) = \sum_{i,j} s_{ij}(\omega) [\mathbf{d}_{21}]_i^* [\mathbf{d}_{21}]_j$ and $S(-\omega) = \sum_{i,j} s_{ij}(-\omega) [\mathbf{d}_{21}]_i [\mathbf{d}_{21}]_j^*$ with the parameter s_{ij} defined by

$$s_{ij}(\omega) = \frac{1}{\hbar^2} P \int_0^\infty d\omega_1 \int_0^\infty d\omega_2 \times \left[\frac{\langle E_i(\mathbf{r}, \omega_2) E_j^\dagger(\mathbf{r}', \omega_1) \rangle}{\omega - \omega_2} + \frac{\langle E_i^\dagger(\mathbf{r}, \omega_2) E_j(\mathbf{r}', \omega_1) \rangle}{\omega + \omega_2} \right], \quad (6)$$

where P is the Cauchy principal value. The Lindblad dissipator

$$\mathcal{D}[\rho(t)] = \Gamma(\omega) [\rho_{22}(t)|1\rangle\langle 1| - \frac{1}{2}\{|2\rangle\langle 2|, \rho(t)\}] + \Gamma(-\omega) [\rho_{11}(t)|2\rangle\langle 2| - \frac{1}{2}\{|1\rangle\langle 1|, \rho(t)\}], \quad (7)$$

contains the downward and upward atomic transitions $\Gamma(\omega) = \sum_{i,j} \gamma_{ij}(\omega) [\mathbf{d}_{21}]_i^* [\mathbf{d}_{21}]_j$ and $\Gamma(-\omega) = \sum_{i,j} \gamma_{ij}(-\omega) [\mathbf{d}_{21}]_i [\mathbf{d}_{21}]_j^*$, where the rates $\gamma_{ij}(\pm\omega)$ are expressed in terms of the Fourier transform of the electric-field correlation functions as follows [64,66]:

$$\gamma_{ij}(\omega) = \frac{2\pi}{\hbar^2} \int_0^\infty d\omega' \times \begin{cases} \langle E_i(\mathbf{r}, \omega) E_j^\dagger(\mathbf{r}, \omega') \rangle, & \omega > 0, \\ \langle E_i^\dagger(\mathbf{r}, -\omega) E_j(\mathbf{r}, \omega') \rangle, & \omega < 0. \end{cases} \quad (8)$$

B. Transition rates out of thermal equilibrium

Based on the canonical quantization scheme, the frequency component of the electric field is given by

$$\mathbf{E}(\mathbf{r}, \omega) = \frac{i\omega^2}{c^2} \sqrt{\frac{\hbar}{\pi\epsilon_0}} \int d^3\mathbf{r}' \sqrt{\text{Im}[\epsilon(\mathbf{r}', \omega)]} \times \bar{\bar{\mathbf{G}}}(\mathbf{r}, \mathbf{r}', \omega) \cdot \mathbf{f}(\mathbf{r}', \omega), \quad (9)$$

where Im stands for the imaginary part and $\bar{\bar{\mathbf{G}}}$ is the electromagnetic Green's tensor fulfilling the Helmholtz equation $[\nabla \times \nabla \times - \epsilon(\omega)\omega^2/c^2] \bar{\bar{\mathbf{G}}}(\mathbf{r}, \mathbf{r}') = \bar{\mathbf{I}}\delta(\mathbf{r} - \mathbf{r}')$ together with the appropriate boundary conditions. Here, $\bar{\mathbf{I}}$ is the unit dyadic.

Using Eqs. (3), (8), and (9), and the Green's identity $\omega^2 \int d^3\mathbf{s} \text{Im}[\epsilon(\mathbf{s}, \omega)] \bar{\bar{\mathbf{G}}}(\mathbf{r}, \mathbf{s}, \omega) \cdot \bar{\bar{\mathbf{G}}}^*(\mathbf{s}, \mathbf{r}', \omega) = c^2 \text{Im}[\bar{\bar{\mathbf{G}}}(\mathbf{r}, \mathbf{r}', \omega)]$, the downward and upward atomic transitions $\Gamma(\omega)$ and $\Gamma(-\omega)$ are written as [64]

$$\begin{pmatrix} \Gamma(\omega_0) \\ \Gamma(-\omega_0) \end{pmatrix} = \Gamma_0 \frac{\rho(\hat{\mathbf{n}}_d, \mathbf{r}_a, \omega_0)}{\rho_0} \begin{pmatrix} 1 + n_{\text{eff}}(\omega_0) \\ n_{\text{eff}}(\omega_0) \end{pmatrix}, \quad (10)$$

where $\Gamma_0 = \frac{\omega_0^3 |\mathbf{d}_{12}|^2}{3\pi\epsilon_0\hbar c^3}$ is the vacuum spontaneous emission rate. Here, the partial local density of states (PLDOS) is defined as [67]

$$\rho(\hat{\mathbf{n}}_d, \mathbf{r}, \omega) = \frac{6\omega}{\pi c^2} (\hat{\mathbf{n}}_d \cdot \text{Im}[\bar{\bar{\mathbf{G}}}(\mathbf{r}, \mathbf{r}, \omega)] \cdot \hat{\mathbf{n}}_d^*), \quad (11)$$

where $\hat{\mathbf{n}}_d$ is a unit vector pointing in the direction of the dipole moment \mathbf{d}_{21} . This quantity, which depends on the material properties of the sphere, the atom position, and the orientation of the atom's dipole moment, measures the number of photonic states per unit of frequency and volume at a certain position and frequency due to the presence of the sphere. In particular, in free space, after averaging Eq. (11) over different dipole orientation, ρ is simply $\rho_0 = \omega_0^2/\pi^2 c^3$. The effective parameter

$$n_{\text{eff}}(\omega_0) = n(\omega_0, T_0) + \frac{\rho_m(\hat{\mathbf{n}}_d, \mathbf{r}_a, \omega_0)}{\rho(\hat{\mathbf{n}}_d, \mathbf{r}_a, \omega_0)} (n(\omega_0, T_1) - n(\omega_0, T_0)), \quad (12)$$

depends both on temperatures and the material properties of the sphere. This material dependence, emerging out of the nonequilibrium configuration of the system, is established through the quantity

$$\rho_m(\hat{\mathbf{n}}_d, \mathbf{r}_a, \omega) = \frac{6\omega^3}{\pi c^4} \int_0^a dr' r'^2 \text{Im}[\epsilon(r', \omega)] \int d\phi' d\theta' \sin\theta' \times (\hat{\mathbf{n}}_d \cdot \bar{\bar{\mathbf{G}}}(\mathbf{r}_a, \mathbf{r}', \omega) \cdot \bar{\bar{\mathbf{G}}}^*(\mathbf{r}', \mathbf{r}_a, \omega) \cdot \hat{\mathbf{n}}_d^*), \quad (13)$$

which from now on we call the medium PLDOS. Likewise, one can define its vacuum counterpart, i.e., $\rho_v(\hat{\mathbf{n}}_d, \mathbf{r}_a, \omega)$, where the lower and upper bounds of the above integral are replaced by a and ∞ , respectively. These two quantities lead to the PLDOS, $\rho = \rho_m + \rho_v$, through the Green's identity. Note that ρ_m and ρ_v are positive quantities since $\text{Im} \epsilon \geq 0$ and their integrals can be recast into a form $\int |g|^2$ using the reciprocity theorem, $\bar{\bar{\mathbf{G}}}_{ij}(\mathbf{r}', \mathbf{r}_a, \omega) = \bar{\bar{\mathbf{G}}}_{ji}(\mathbf{r}_a, \mathbf{r}', \omega)$. With this

in mind, the effective parameter (12) can be rearrange to give $n_{\text{eff}} = (n(\omega, T_0)\rho_v + n(\omega, T_1)\rho_m)/\rho$, resulting in the inequality $n(\omega, T_{\min}) \leq n_{\text{eff}} \leq n(\omega, T_{\max})$ where $T_{\min} = \min(T_0, T_1)$ and $T_{\max} = \max(T_0, T_1)$. Subsequently, the downward and upward atomic transitions (10) are bounded between their equilibrium counterpart values at temperatures T_0 and T_1 . These findings are in agreement with the results reported in Ref. [43].

In the case $T_1 = T_0 = T$, the sphere is in the thermal equilibrium with the background thermal radiations and $n_{\text{eff}}(\omega_0)$ reduces to the mean thermal photon number $n(\omega_0, T)$. Therefore, the atomic transitions $\Gamma(\pm\omega_0)$ are expressed as a product of $\Gamma_0\rho/\rho_0$ with the factor $1 + n(\omega_0, T)$ or $n(\omega_0, T)$ at the thermal equilibrium, as expected.

Given these results, the dynamic evolution of the elements of the reduced atomic density operator (4) can be written as

$$\dot{\varrho}_{11}(t) = -\Gamma(-\omega_0)\varrho_{11}(t) + \Gamma(\omega_0)\varrho_{22}(t), \quad (14a)$$

$$\dot{\varrho}_{22}(t) = \Gamma(-\omega_0)\varrho_{11}(t) - \Gamma(\omega_0)\varrho_{22}(t), \quad (14b)$$

$$\dot{\varrho}_{12}(t) = \left[i(\Lambda + \omega_0) - \frac{\Gamma(\omega_0) + \Gamma(-\omega_0)}{2} \right] \varrho_{12}(t), \quad (14c)$$

where $\Lambda \equiv \Omega - \omega_0$ is the so-called Lamb shift. Using Eqs. (6) and (9) and the Kramers-Kronig relations the Lamb shift is given by

$$\Lambda(\omega_0) = -\frac{\omega}{\hbar\epsilon_0 c^2} (\hat{\mathbf{n}}_d \cdot \text{Re}[\bar{\mathbf{G}}(\mathbf{r}_a, \mathbf{r}_a, \omega_0)] \cdot \hat{\mathbf{n}}_d^*), \quad (15)$$

which is independent of the temperatures. This implies that the Lamb shift does not depend on the absence or presence of thermal equilibrium.

III. GEOMETRIC PHASE

In this section, we turn to compute the GP associated with the evolution of the two-level atom in a stationary configuration out of thermal equilibrium. It is well known that the atom evolves nonunitarily due to its coupling with the medium-assisted electromagnetic field near the nanosphere whose temperature is kept fixed and different from that of the surrounding vacuum. We pursue the kinematic approach of Tong *et al.* [21], which gives the GP for a quantum system under nonunitary dynamical evolution, and it reads

$$\Phi = \arg \sum_k \sqrt{\varepsilon_k(0)\varepsilon_k(t)} \langle \psi_k(0) | \psi_k(t) \rangle e^{-\int_0^t dt' \langle \psi_k(t') | \dot{\psi}_k(t') \rangle}, \quad (16)$$

where $\varepsilon_k(t)$ and $|\psi_k(t)\rangle$ are the eigenvalues and eigenvectors of the reduced density matrix $\varrho(t)$. As can be seen from the definition above, to compute the GP, it is important to first find the solution of time-dependent reduced density matrix (14) at all times. To this end, we assume that the atom is initially

prepared in a superposition of upper and lower states in a Ramsey zone

$$|\psi(0)\rangle = \cos \frac{\theta_0}{2} |2\rangle + \sin \frac{\theta_0}{2} |1\rangle, \quad (17)$$

where θ_0 can be controlled by the time duration of a laser pulse that is irradiated on the atom [19,68,69]. Using Eqs. (14), the elements of reduced density matrix for times $t > 0$ are given by

$$\varrho_{11}(t) = \sin^2 \frac{\theta_0}{2} e^{-\Gamma_+ t} + \frac{\Gamma_+ + \Gamma_-}{2\Gamma_+} (1 - e^{-\Gamma_+ t}), \quad (18a)$$

$$\varrho_{22}(t) = \cos^2 \frac{\theta_0}{2} e^{-\Gamma_+ t} + \frac{\Gamma_+ - \Gamma_-}{2\Gamma_+} (1 - e^{-\Gamma_+ t}), \quad (18b)$$

$$\varrho_{12}(t) = \varrho_{21}^*(t) = \frac{1}{2} e^{i(\Omega - \Gamma_+/2)t} \sin \theta_0, \quad (18c)$$

where $\Gamma_{\pm} \equiv \Gamma(\omega_0) \pm \Gamma(-\omega_0)$, with Γ_+ being the dephasing decay rate of the quantum coherence of the system. Solving the eigenvalue problem for the reduced density matrix, the eigenvalues of $\varrho(t)$ are obtained as

$$\begin{aligned} \varepsilon_{\pm}(t) &= \frac{1}{2} (1 \pm \sqrt{\sin^2 \theta_0 e^{-\Gamma_+ t} + [\cos \theta_0 e^{-\Gamma_+ t} - Q(1 - e^{-\Gamma_+ t})]^2}), \\ & \quad (19) \end{aligned}$$

with $Q \equiv \Gamma_-/\Gamma_+$. The corresponding eigenvectors of $\varrho(t)$ can be expressed as

$$|\psi_+(t)\rangle = e^{i\Omega t} \cos \frac{\theta_t}{2} |1\rangle + \sin \frac{\theta_t}{2} |2\rangle, \quad (20)$$

$$|\psi_-(t)\rangle = e^{i\Omega t} \sin \frac{\theta_t}{2} |1\rangle - \cos \frac{\theta_t}{2} |2\rangle, \quad (21)$$

where $\tan(\theta_t/2) = \sqrt{(\varrho_{22} - \varepsilon_-)/(\varrho_{11} - \varepsilon_-)}$. Since $\varepsilon_-(0) = 0$, we only need $|\psi_+(t)\rangle$ to calculate the GP. Substituting Eqs. (19) and (20) into Eq. (16), the GP reduces to

$$\Phi = \arg \langle \psi_k(0) | \psi_k(t) \rangle - \Omega \int_0^t dt' \cos^2(\theta_{t'}/2). \quad (22)$$

Here, the first term is the Pancharatnam phase [1], which results from the correlation of the time-evolved state $|\psi_k(t)\rangle$ and the initial state $|\psi_k(0)\rangle$, is written by

$$\arg \langle \psi_k(0) | \psi_k(t) \rangle = \frac{\sin \Omega t}{\cos \Omega t + \tan(\theta_t/2) \coth(\theta_t/2)}. \quad (23)$$

For the case that the system evolves along a quasicyclic path with the evolution time $t = 2\pi/\Omega$, the Pancharatnam phase (23) vanishes and makes no contribution to the GP. The last term in Eq. (22) arising from the GP of the dynamical evolution, is given by

$$\Phi = -\frac{\Omega}{2} \int_0^T dt \left(1 - \frac{Q - Qe^{\Gamma_+ t} + \cos \theta_0}{\sqrt{\sin^2 \theta_0 e^{\Gamma_+ t} + (Q - Qe^{\Gamma_+ t} + \cos \theta_0)^2}} \right). \quad (24)$$

A direct calculation of this integral is rather tedious. However, a simple estimate can reveal that the ratio Γ_0/ω_0 is vanishingly

small. For instance, considering a free space qubit with the transition frequency $\omega_0/2\pi = 4.68$ GHz and the relaxation

time $2.65 \mu\text{s}$ [69], Γ_0/ω_0 is of order 10^{-5} . This allows us to evaluate this integral by making a series expansion of the integrand in terms of Γ_0/ω_0 . Up to leading order in Γ_0/ω_0 , it leads to

$$\Phi \approx -\pi(1 - \cos \theta_0) - \frac{\Omega}{2\omega_0} \Gamma_0 \sin^2 \theta_0 \int_0^T dt t(2Q + \cos \theta_0) \times \frac{\partial \Gamma +}{\partial(\Gamma_0/\omega_0)}. \quad (25)$$

The first term of Eq. (25) is the GP for the isolated system with no influence from the environment, and the second term is the correction originates from the atom-electromagnetic field interaction in the absence of thermal equilibrium. Using the definition (10) for $\Gamma(\pm\omega_0)$, the GP (25) can be rearranged to give

$$\Phi \approx -\pi(1 - \cos \theta_0) - \frac{\pi^2 \Gamma_0}{2\rho_0 \omega_0} \rho(\hat{\mathbf{n}}_d, \mathbf{r}_a, \omega_0) \sin^2 \theta_0 \times [\cos \theta_0 + 2n_{\text{eff}}(\omega_0) \cos \theta_0 + 2]. \quad (26)$$

As can be seen, in the absence of the electromagnetic modes of the free space and the background thermal radiations, we can recover the familiar expression $\Phi_0 \approx -\pi(1 - \cos \theta_0)$ for the GP [19,22,30]. In what follows, we separate the contribution induced by equilibrium and nonequilibrium effects in the presence of dielectric nanosphere from that of Φ_0 as

$$\Delta \Phi = \frac{\pi^2 \Gamma_0}{2\rho_0 \omega_0} \rho(\hat{\mathbf{n}}_d, \mathbf{r}_a, \omega_0) \sin^2 \theta_0 \times [\cos \theta_0 + 2n_{\text{eff}}(\omega_0) \cos \theta_0 + 2], \quad (27)$$

where $\Delta \Phi = |\Phi - \Phi_0|$. This GP difference reflects the correction to the unitary GP. However, the roles of material and geometrical parameters of the medium and the nonequilibrium effects of the system on $\Delta \Phi$ are ambiguous. A detailed analysis of the GP will follow in the next section, but it would be instructive to study approximate cases as a consistency check and as a useful point of comparison later on. In the small-sphere limit $|k_1 a|, |k_0 a| \ll 1$, where the atom can be very far from or very close to the sphere (see Appendix B), one can gain a simple physical insight into the GP corrections. We first consider the atom-sphere distances $z_a = r_a - a$ to be much smaller than the atomic transition wavelengths, i.e., the atom is located at a position very close to the sphere. In this short-distance limit, $|k_0 r_a| \ll 1$, the sphere facing the atom effectively behaves like a plane. Substituting Eqs. (A4) and (A5) into Eqs. (12) and (27), we derive after some algebra

$$\Delta \Phi \simeq \frac{\pi^2 \Gamma_0}{2\omega_0} \left(1 + \frac{3}{8k_0^3} \text{Im} \left[\frac{\epsilon - 1}{\epsilon + 1} \right] z_a^{-3} \right) \sin^2 \theta_0 \times [2 + \cos \theta_0 + 2n(\omega_0, T_0) \cos \theta_0] + \frac{3\pi^2 \Gamma_0}{4\omega_0 k_0^3} \text{Im}[\epsilon(\omega)] \left| \frac{1}{\epsilon + 1} \right|^2 z_a^{-3} \sin^2 \theta_0 \cos \theta_0 \times [n(\omega_0, T_1) - n(\omega_0, T_0)]. \quad (28)$$

Here, the GP difference exhibits a distance dependence of z_a^{-3} , which is the same as the results of a perfectly conducting plate at zero temperature [70,71]. Furthermore, it has a resonant response when $\text{Re}[\epsilon(\omega)] = -1$. This is properly the resonant

frequency at which surface modes are excited on a flat surface [72].

In the opposite limit of the atom far away from the sphere, $r_a \gg a$, inserting Eqs. (A4) and (A5) into Eqs. (12) and (27), the GP difference reduces to

$$\Delta \Phi \simeq \frac{\pi^2 \Gamma_0}{2\omega_0} \left(1 + \frac{6a^3}{k_0} \text{Im} \left[\frac{\epsilon - 1}{\epsilon + 2} \right] r_a^{-4} \right) \sin^2 \theta_0 \times [2 + \cos \theta_0 + 2n(\omega_0, T_0) \cos \theta_0] + \frac{18\pi^2 a^3 \Gamma_0}{\omega_0 k_0} \text{Im}[\epsilon(\omega)] \left| \frac{1}{\epsilon + 2} \right|^2 r_a^{-4} \sin^2 \theta_0 \cos \theta_0 \times [n(\omega_0, T_1) - n(\omega_0, T_0)], \quad (29)$$

where, unlike the short distance limit, it shows a distance dependence of r_a^{-4} and becomes significant at the resonance frequency at which $\text{Re}[\epsilon(\omega)] = -2$. As explained in the next section, this occurs for spherical structures that support plasmonic or phononic modes.

For most metals, the resonance frequency of plasmonic mode lies in the near UV and visible range so that these surface waves are difficult to excite thermally. By contrast, surface-phonon polaritons mode can be excited thermally because they exist in the infrared. Therefore, in what follows, we only concentrate on the dielectric sphere.

IV. NUMERICAL ANALYSIS

In this section, we present a numerical analysis of the GP (27) for the case where the atom is located on the z axis at a distance of $r_a = 1.7 \mu\text{m}$ from the center of a nanosphere with the radius of $a = 700 \text{ nm}$ for both out-of-thermal equilibrium and in-thermal equilibrium configurations. We consider the dipole moment of the atom oriented perpendicularly to the surface of the GaAs nanosphere, i.e., $\hat{\mathbf{n}}_d = \hat{\mathbf{r}}$. Similar results are obtained for the case where the dipole moment of the atom is tangent to the surface of the nanosphere (not shown here). Here, the gallium arsenide (GaAs) nanosphere is investigated, which supports surface waves known as localized surface phonon-polaritons (LSPPhP), with optical properties well described by the Drude-Lorentz model

$$\epsilon(\omega) = \epsilon_\infty \frac{\omega^2 - \omega_l^2 + i\gamma_e \omega}{\omega^2 - \omega_r^2 + i\gamma_e \omega}, \quad (30)$$

where $\epsilon_\infty = 11$, $\gamma_e = 0.00452 \times 10^{14} \text{ (rad/s)}$, $\omega_r = 0.506 \times 10^{14} \text{ (rad/s)}$, and $\omega_l = 0.550 \times 10^{14} \text{ (rad/s)}$ [73]. The GaAs nanosphere embedded in a vacuum exhibits a dipolar surface-phonon mode at a frequency dictated by the condition $\text{Re}[\epsilon(\omega)] = -2$ [72]. Using the Drude-Lorentz model (30), this resonance appears at the frequency of $1.074\omega_r$. In what follows, we assume that the atomic frequencies are of the same order as the resonance frequency of the sphere. Such frequencies can be achievable using artificial atoms made of semiconductor quantum dots [74].

A. Medium-induced corrections to the GP difference

In this subsection, we restrict our attention to the GP difference alone due to the presence of the nanosphere. To this end, we consider that the whole system is in thermal equilibrium

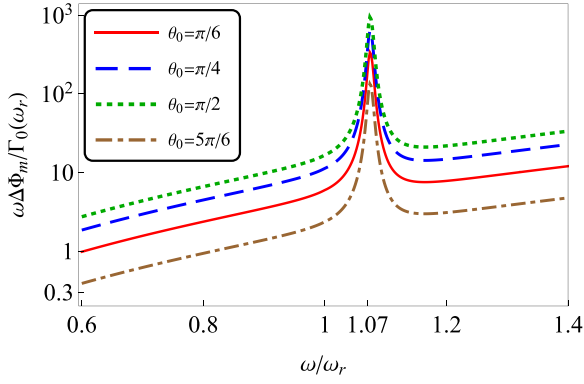


FIG. 2. The normalized medium-induced GP $\omega\Delta\Phi_m/\Gamma_0(\omega_r)$ versus normalized frequency ω/ω_r for four initial states of $\theta_0 = \pi/6$ (red solid line), $\theta_0 = \pi/4$ (blue dashed line), $\theta_0 = \pi/2$ (green dotted line), and $\theta_0 = 5\pi/6$ (brown dot-dashed line). The nanosphere is made of GaAs with the permittivity function (30). The atom is located on the z axis at a distance of $r_a = 1.7\mu\text{m}$ from the center of the GaAs nanosphere with the radius of $a = 700\text{nm}$.

at zero temperature. For this particular case of zero temperature, due to Eq. (12), n_{eff} vanishes and the medium-induced correction to the GP (27) is obtained as

$$\Delta\Phi_m = \frac{\pi^2\Gamma_0}{2\rho_0\omega_0} \rho(\hat{\mathbf{r}}, \mathbf{r}_a, \omega_0) \sin^2\theta_0[\cos\theta_0 + 2], \quad (31)$$

which depends on the properties of the atom via the transition frequency ω_0 and the spontaneous emission in vacuum Γ_0 , the initial state θ_0 , and material and geometrical properties of the nanosphere through ρ . In the absence of the dielectric sphere, where $\rho = \rho_0$, the GP difference (31) reduces to $\pi^2\Gamma_0 \sin^2\theta_0[2\cos\theta_0 + 1]/\omega_0$, which is just the GP difference acquired by a two-level atom in a vacuum. This is consistent with the result obtained for a two-level atom coupled to an environment with Lorentzian spectral density [30]. However, as depicted in Fig. 2, the presence of the sphere disrupts this result due to supporting surface-phonon modes. This figure illustrates the normalized medium-induced GP, $\omega\Delta\Phi_m/\Gamma_0(\omega_r)$, as a function of normalized frequency ω/ω_r for different initial states of θ_0 . The GP difference, which is proportional to the PLDOS, shows a peak at $\omega = 1.074\omega_r$ that corresponds to the LSPHP resonance. This increases the PLDOS close to the sphere, which leads to a significant GP difference and provides ideal conditions for GP detection. It further shows that the GP difference enhances as θ_0 increases from zero to $\pi/2$, while it decreases as θ_0 increases beyond $\pi/2$. This is understandable because the maximum of $\Delta\Phi_m$ occurs around $\theta_0 = \pi/2$ with the maximum medium-induced GP $\pi^2\Gamma_0\rho(\omega_0)/\rho_0\omega_0$ where Φ_0 also reaches its maximum, whereas $\Delta\Phi_m$ vanishes when $\theta_0 = 0$ and $\theta_0 = \pi$. Figure 3 shows that the damping coefficient γ_e can significantly influence on the medium-induced GP difference. The GP difference is always larger than that in the absence of the nanosphere at given frequencies, so that it is more pronounced in the LSPHP resonance. Furthermore, the peak width becomes broader with increasing γ_e because the linewidth of the PLDOS is closely associated with the damping coefficient. In this sense, the dissipative effect of

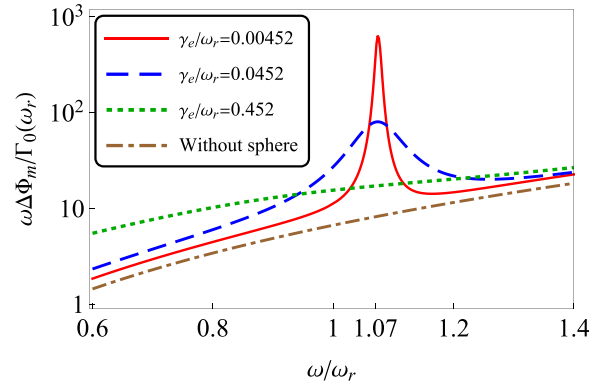


FIG. 3. The normalized medium-induced GP $\omega\Delta\Phi_m/\Gamma_0(\omega_r)$ versus the normalized frequency ω/ω_r for three values of the damping coefficient $\gamma_e = 0.00452\omega_r$ (red solid line), $\gamma_e = 0.0452\omega_r$ (blue dashed line), and $\gamma_e = 0.452\omega_r$ (green dotted line). As a reference, the GP difference in the absence of the nanosphere is plotted by the brown dot-dashed line. Here, $\theta_0 = \pi/4$, and other parameters are the same as those in Fig. 2.

the sphere has a strong correction around the LSPHP frequency. Far from the LSPHP resonance, the GP difference is relatively small, but it increases slightly for larger values of γ_e . Since the PLDOS contains two radiative and nonradiative channels through which the atom can decay, therefore, this enhancement can be attributed to the increase in the non-radiative decay to the absorption modes in the nanosphere. Interestingly, our result indicates the insensitivity of the GP to the presence of the nanosphere far from (near) the LSPHP resonance frequency when the absorption is weak (strong). This means that the GP difference shows a stronger resilience to the medium with a large γ_e near the LSPHP resonance frequency. To make this clear, let us derive an approximate expression for the medium-induced GP in the small-sphere limit where the atom is far from the sphere. By making use of Eq. (29), after some manipulations, we get

$$\Delta\Phi_m \simeq \frac{\pi^2\Gamma_0}{2\omega_0} \left(1 + \frac{18a^3 \text{Im}[\epsilon] r_a^{-4}}{k_0((\text{Re}[\epsilon] + 2)^2 + (\text{Im}[\epsilon])^2)} \right) \times \sin^2\theta_0[2 + \cos\theta_0]. \quad (32)$$

It is clear that the imaginary part of the permittivity function in the denominator of the above equation suppresses the GP divergence at the resonant frequency, particularly when the damping coefficient is too large. Consequently, it is expected that the peak at $\omega = 1.074\omega_r$ gradually disappears with increasing absorption (see Fig. 3), and exhibits a strong robustness to high absorption at the resonance frequency. The robustness features of GP in the presence of dissipation can be an important resource for the construction of phase gates [75] in quantum information systems.

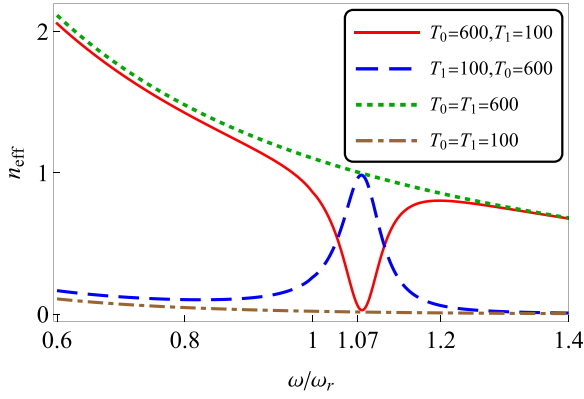


FIG. 4. The effective parameter n_{eff} versus the normalized frequency ω/ω_r . Two configurations out of thermal equilibrium with temperatures $T_0 = 600$ K, $T_1 = 100$ K (red solid line) and $T_0 = 100$ K, $T_1 = 600$ K (blue dashed line) are compared with thermal equilibrium configurations at temperatures $T_0 = T_1 = 600$ K (green dotted line) and $T_0 = T_1 = 100$ K (brown dot-dashed line). The parameters we chose are the same as those in Fig. 2.

B. Out of thermal equilibrium induced corrections to the GP in the presence of the nanosphere

In the following, we mainly concentrate on out of thermal equilibrium corrections to the GP defined as

$$\Delta\Phi_{\text{out-eq}} = \frac{\pi^2\Gamma_0}{\rho_0\omega_0}\rho(\hat{\mathbf{r}}, \mathbf{r}_a, \omega_0)n_{\text{eff}}(\omega_0)\sin^2\theta_0\cos\theta_0, \quad (33)$$

where the material property of the nanosphere is encoded on both quantities ρ and n_{eff} . Likewise, the thermal equilibrium corrections to the GP, i.e., $\Delta\Phi_{\text{eq}}$, can be obtained by replacing n_{eff} in the above equation with the mean thermal photon number n . Figure 4 indicates the temperature and frequency dependence of n_{eff} , appearing in Eq. (33), for two configurations out of thermal equilibrium at $T_0 = 600$ K, $T_1 = 100$ K and $T_0 = 100$ K, $T_1 = 600$ K, and compares them with the corresponding thermal-equilibrium parameter, i.e., n , at temperatures $T_0 = T_1 = T_{\text{max}} = 600$ K and $T_0 = T_1 = T_{\text{min}} = 100$ K. It is observed that n_{eff} is enclosed between $n(\omega, T_{\text{min}})$ and $n(\omega, T_{\text{max}})$, which is also established in Sec. II, and shows a significant variations around the LSPHP resonance. As a consequence, the GP difference $\Delta\Phi_{\text{out-eq}}$, which is proportional to n_{eff} , is always bounded between the thermal-equilibrium counterparts $\Delta\Phi_{\text{eq}}(T_{\text{min}})$ and $\Delta\Phi_{\text{eq}}(T_{\text{max}})$, as shown in Fig. 5. In Fig. 5(a), the GP difference as a function of the frequency follows similar variations both in thermal equilibrium and out of thermal equilibrium, showing a strong peak around the LSPHP resonance. However, the peak height is almost small when the nanosphere is at a lower temperature than the vacuum environment, although it is still larger than the thermal-equilibrium configuration at the sphere temperature [compare the red solid and brown dot-dashed lines in Fig. 5(a)]. This is because, for the small atom-sphere separations considered here, the temperature of the sphere plays a significant role in the GP difference at the resonance frequency. It is evident from Fig. 5(b) that for small values of the dimensionless distance $\omega_r r/c$ only the temperature of the nanosphere contributes, while at intermediate atomic

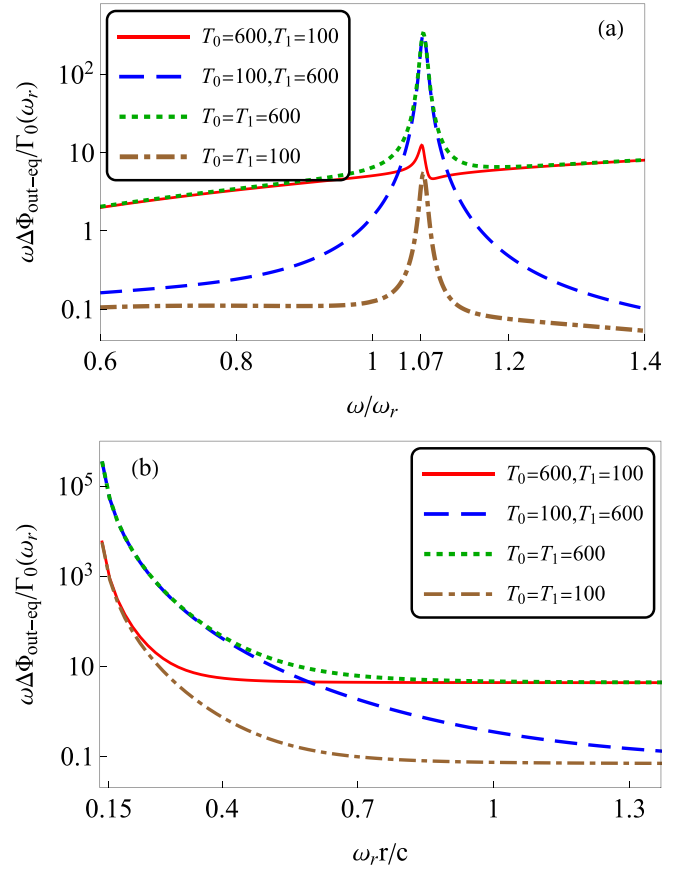


FIG. 5. The normalized GP deviation $\omega\Delta\Phi_{\text{out-eq}}/\Gamma_0(\omega_r)$ versus the (a) normalized frequency ω/ω_r and (b) the normalized distance $\omega_r r/c$ for both in thermal equilibrium and out of thermal equilibrium configurations. In (a), $r_a = 1.7\mu\text{m} = 0.29c/\omega_r$, and in (b) $\omega = 1.074\omega_r$. The other parameters are the same as in Figs. 2 and 4.

distances both sphere and vacuum temperatures play a role in the GP difference. In contrast, for large values of $\omega_r r/c$, the out of thermal equilibrium induced GP tends towards the equilibrium counterpart at the vacuum temperature. This means that at large distances, only the vacuum temperature affects the GP difference. Therefore, at large (small) atomic distances, the GP difference at the LSPHP resonance can vary with the temperature of the vacuum (sphere).

C. Total corrections to the GP in the presence of the nanosphere

In this subsection, we consider the combination of both medium and out of thermal equilibrium corrections to the GP in the presence of the nanosphere. Figure 6 shows the sum of these corrections, i.e., Eq. (27), as a function of the dimensionless frequency ω/ω_r . We compare the GP difference at thermal equilibrium at $T_0 = T_1 = 100$ K and $T_0 = T_1 = 600$ K with the GP out of thermal equilibrium at $T_0 = 600$ K, $T_1 = 100$ K and $T_0 = 100$ K, $T_1 = 600$ K. As a reference, the GP difference is also plotted in the absence of the nanosphere at the vacuum environment temperature of 100 K (the black dotted line). As can be seen, the GP deviation $\Delta\Phi$ shows a considerable increase at the LSPHP resonance for both in thermal and out of thermal equilibrium. However, regardless

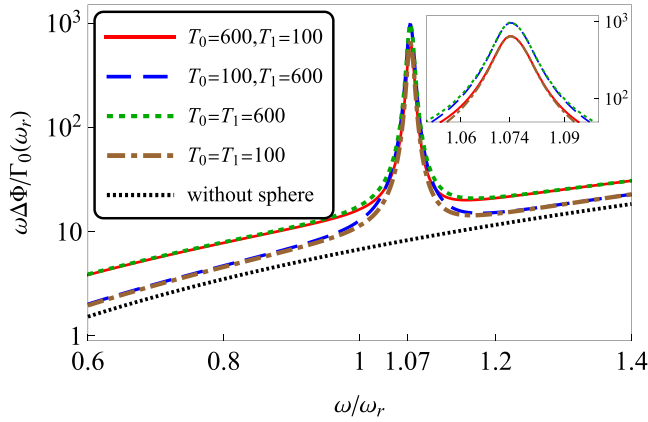


FIG. 6. The normalized total GP deviation $\omega\Delta\Phi/\Gamma_0(\omega_r)$ as a function of the normalized frequency ω/ω_r for both in thermal equilibrium and out of thermal equilibrium configurations. The black dotted line shows the GP difference in the absence of the nanosphere at the vacuum temperature of 100 K. Here, $\theta_0 = \pi/4$, and other parameters are the same as in Figs. 2 and 4. The inset shows the zoomed region near the LSPHP resonance.

of the temperature of the sphere and the environment, there is a slight difference between these curves for the atom distance considered here. This is due to the prominent role of the medium-induced correction to the GP at the LSPHP frequency and demonstrates almost the robustness of the GP to the temperature difference of the sphere and the environment. Far from the LSPHP resonance, the GP difference decreases sharply for out of thermal equilibrium configurations and approaches the equilibrium counterparts at the vacuum environmental temperatures. In this sense, a small variation of frequency around the LSPHP resonance lead to drastically modifications of the GP difference. This can provide evidence of thermally excited surface evanescent waves. In Fig. 7, the

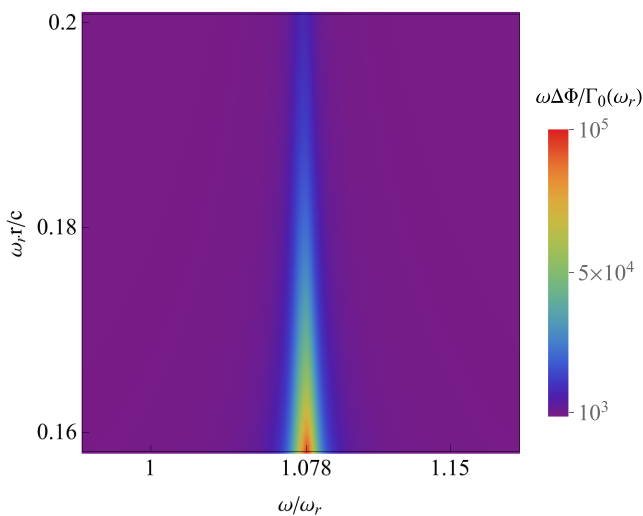


FIG. 7. Density plot of the GP deviation $\Delta\Phi$ as functions of the normalized distance $\omega_r r/c$ and the normalized frequency ω/ω_r for out of thermal equilibrium configuration with temperature $T_0 = 600$ K, $T_1 = 100$ K. Here, $\theta_0 = \pi/4$, and the other parameters are the same as in Fig. 2.

GP difference $\Delta\Phi$ is shown as a function of the dimensionless frequency ω/ω_r and the dimensionless distance $\omega_r r/c$ for $T_0 = 600$ K and $T_1 = 100$ K. This illustrates the role of LSPHP resonance in the GP difference. In particular, it exhibits a peak centered at the frequency $\omega = 1.078\omega_r$ for a very small atom-sphere distance. Recalling Eq. (32), we find that this frequency is the resonance frequency of surface modes in a plane, which estimated from the relation $\text{Re}[\epsilon(\omega)] = -1$. Close to the nanosphere, the PLDOS increases in the presence (absence) of evanescent surface waves confined near the surface of the sphere and strongly enhances (decreases) the GP difference. Far from the nanosphere, the PLDOS decreases due to the absence of evanescent radiation, resulting in a decrease in the GP difference. These results still hold when the sphere radius is increased and the atom-sphere distance is kept constant (not shown here).

D. Experimental proposal

According to the obtained results, we conclude that the model under study is a suitable scheme for measuring the GP in nonequilibrium thermal conditions. In what follows, we present two experimental proposals to account for sphere-induced corrections and thermal equilibrium effects on the GP. Our first scheme for measuring the GP relies on the use of a single nitrogen-vacancy (NV) center in diamond as an effective two-level system [76]. It can be attached to the tip of an atomic force microscope (AFM) and placed at the distance z_a of the surface of a dielectric sphere. With the ability to maintain the distance between the NV center and the sphere, this AFM can provide a good strategy to realize subnanometer resolution [40]. Since, for a fixed atom-sphere distance and a specific frequency the GP correction is maximized when $\theta_0 = \pi/2$ (see Sec. IV A), the atom can be prepared in an equal superposition between the upper and lower states. A dielectric sphere made of GaAs with a temperature different from the environment is used. We follow the scheme introduced in Refs. [40,77] and extract the GP in a tomographic manner by measuring elements of the reduced density matrix of the atom and numerical interpolation of these elements in Eq. (22). Consider an NV center with the transition frequency of $\omega_0/2\pi = 54.3$ THz and a lifetime of ~ 1 ns, which is accessible with current technology facilities [78,79] and is in resonant with the sphere. When the NV center is at a distance of 100 nm from the surface of the sphere, and the sphere is heated to $T_1 = 320$ K with the ambient temperature at room temperature, one can reach the total GP difference of ~ 0.57 rad.

In the second scenario, the GP acquired by the atom can be detected with an atom interferometer in which two atoms follow two different paths [41,80]. In one path, the atom moves through a cavity with walls at temperature T_0 containing a sphere at temperature T_1 . The sphere lies in the vicinity of the path in black-body radiation emitted from the cavity far from the sphere. This system can be equivalently interpreted in terms of a system in thermal equilibrium with an effective temperature, $T_{\text{eff}} = \hbar\omega_0[k_B \ln(1 + n_{\text{eff}})]^{-1}$ whose value depends on the geometry of the sphere, the sphere-atom distance, and optical resonances [43]. In the second path, another atom as a reference atom passes through a cavity

with the same temperature and characteristics as the first arm, which is now empty of the sphere. In both paths, the atoms acquire GP due to the interaction with the thermal field and the near field of the sphere, and their motions. The atoms of the two paths meet at the output, and in this way, the thermal equilibrium and motion corrections to the GP between the two interferometer arms can be eliminated. Although we use moving atoms, but for small values of the velocity the correction of the GP is mainly induced by the presence of the thermal field and dielectric sphere [40]. Out-of-thermal equilibrium correction to the GP are measured by a shift in the interference fringes at the output. Note that the trajectories can be chosen such that the dynamic relative phases cancel [41]. Inspired by Ref. [41], this design for GP detection can be used to build a high precision quantum thermometer. Although, this atomic interferometer can be prepared in a different way, so that all the equipment is placed, for example, at room temperature, and the sphere is heated or cooled at a different temperature T_1 .

V. CONCLUSION

We studied the corrections to the GP under a nonunitary evolution induced by the presence of a dielectric nanosphere. We considered the atom to be embedded in a stationary configuration out of thermal equilibrium, where the medium temperature is kept fixed and different from the surrounding free space. The effect of optical and geometrical properties of the dielectric medium along with its temperature on the geometric phase has been explored analytically and numerically. It was demonstrated that the first-order correction to the GP, which is proportional to the partial local density of states and the effective parameter n_{eff} is significantly large close to the nanosphere when the surface phonon modes excited. In this sense, a small change in frequency around the resonance frequency leads to drastic changes in the GP, providing ideal conditions for the GP detection.

However, the GP has shown a stronger resilience to the medium with a large damping coefficient near the localized surface phonon-polaritons resonance frequency. For the small atom-sphere separations, the medium temperature leaves its footprint in the GP acquired by the atom, while for large distances, the sphere temperature is immaterial, and the out-of-thermal equilibrium-induced GP approaches the equilibrium counterpart at the free space temperature. This suggests that the geometric phase can be used to construct a quantum thermometer for dielectric media in the nonequilibrium regime. Our results beautifully demonstrate properties of the GP near material media that support phononic or even plasmonic modes both in thermal and out of thermal equilibrium configurations and serve as a stepping stone for further research of GP as a resource for quantum computation or quantum sensing.

APPENDIX A: GREEN'S TENSOR OF THE SYSTEM

Following the method of scattering superposition in Refs. [62,63,81], we can write the electromagnetic Green's tensor of the nanosphere in Fig. 1 in the form $\bar{\bar{\mathbf{G}}}(\mathbf{r}, \mathbf{r}', \omega) = \bar{\bar{\mathbf{G}}}_0(\mathbf{r}, \mathbf{r}', \omega)\delta_{fs} + \bar{\bar{\mathbf{G}}}_s^{(fs)}(\mathbf{r}, \mathbf{r}', \omega)$, where $\bar{\bar{\mathbf{G}}}_0$ denotes the con-

tribution of the direct waves from the emitter in an unbounded vacuum, the scattering Green's tensor $\bar{\bar{\mathbf{G}}}_s^{(fs)}$ describes the multiple reflection and transmission processes due to the interaction of the emitter with the nanosphere, f and s refer to the regions where the field point and source point are located, and δ_{fs} is the usual Kronecker delta. In the current study, the atom (emitter) is located out of the nanosphere on the z axis. This, together with the analysis of Eqs. (11) to (13), leads us to the fact that the field (source) point is placed outside (both outside and inside) of the nanosphere. Since the dipole moment of the atom is along the radial direction, i.e., $\hat{\mathbf{r}}$, only the radial component of the direct term of the Green's function is needed to compute the PLDOS, which is given by

$$\bar{\bar{\mathbf{G}}}_{0,rr}(\mathbf{r}_a, \mathbf{r}_a, \omega) = \frac{ik_0}{4\pi} \sum_n n(n+1)(2n+1) \times \frac{h_n^{(1)}(k_0 r_a) j_n(k_0 r_a)}{(k_0 r_a)^2}. \quad (\text{A1})$$

While, for the scattered part, the following components are required in the PLDOS and ρ_m calculations:

$$\bar{\bar{\mathbf{G}}}_{s,rr}^{(00)}(\mathbf{r}_a, \mathbf{r}_a, \omega) = \frac{ik_0}{4\pi} \sum_n n(n+1)(2n+1) B_N^{00}(\omega) \times \left(\frac{h_n^{(1)}(k_0 r_a)}{k_0 r_a} \right)^2, \quad (\text{A2a})$$

$$\bar{\bar{\mathbf{G}}}_{s,rr}^{(01)}(\mathbf{r}_a, \mathbf{r}', \omega) = \frac{ik_1}{4\pi} \sum_n n(n+1)(2n+1) A_N^{01}(\omega) \times \left(\frac{h_n^{(1)}(k_0 r_a) j_n(k_1 r')}{k_0 r_a k_1 r'} \right) P_n(\cos \theta'), \quad (\text{A2b})$$

$$\bar{\bar{\mathbf{G}}}_{s,r\theta}^{(01)}(\mathbf{r}_a, \mathbf{r}', \omega) = \frac{ik_1}{4\pi} \sum_n (2n+1) A_N^{01}(\omega) \times \left(\frac{h_n^{(1)}(k_0 r_a) \partial j_n(k_1 r')}{k_0 r_a k_1 r'} \right) \frac{dP_n(\cos \theta')}{d\theta'}, \quad (\text{A2c})$$

$$\bar{\bar{\mathbf{G}}}_{s,r\varphi}^{(01)}(\mathbf{r}_a, \mathbf{r}', \omega) = 0, \quad (\text{A2d})$$

where $k_0 = \omega/c$, $k_1 = \sqrt{\epsilon} \omega/c$, and the prime in the last three equations represents the coordinates (r', θ', φ') of the source inside the sphere. Here, $j_n(x)$ is the spherical Bessel function of the first kind, $h_n^{(1)}(x)$ is the first-type of spherical Hankel function, and $P_n^m(x)$ is the associated Legendre function.

The scattering coefficients $B_N^{00}(\omega)$ and $A_N^{01}(\omega)$ in Eqs. (A2) are related to the reflection and transmission coefficients $-R_{F0}^V(\omega)$ and $T_{F0}^V(\omega)$, respectively, with

$$R_{F1}^V = \frac{k_1 j_n(k_1 a) \partial j_n(k_0 a) - k_0 j_n(k_0 a) \partial j_n(k_1 a)}{k_1 j_n(k_1 a) \partial h_n^{(1)}(k_0 a) - k_0 \partial j_n(k_1 a) h_n^{(1)}(k_0 a)}, \quad (\text{A3a})$$

$$T_{F1}^V = \frac{k_1 (j_n(k_1 a) \partial h_n^{(1)}(k_1 a) - \partial j_n(k_1 a) h_n^{(1)}(k_1 a))}{k_1 j_n(k_1 a) \partial h_n^{(1)}(k_0 a) - k_0 \partial j_n(k_1 a) h_n^{(1)}(k_0 a)}, \quad (\text{A3b})$$

where we introduced the abbreviations $\partial j_n(x) = \frac{1}{x} \frac{d[x j_n(x)]}{dx}$ and $\partial h_n^{(1)}(x) = \frac{1}{x} \frac{d[x h_n^{(1)}(x)]}{dx}$.

Inserting Eqs. (A1) and (A2a) into Eq. (11), after some manipulations, the PLDOS is rewritten as

$$\rho(\hat{\mathbf{r}}, \mathbf{r}_a, \omega) = \rho_0 \left[1 + \frac{3}{2} \text{Re} \sum_n n(n+1)(2n+1) B_N^{00}(\omega) \times \left(\frac{h_n^{(1)}(k_0 r_a)}{k_0 r_a} \right)^2 \right]. \quad (\text{A4})$$

Likewise, substituting Eqs. (A2b) to (A2d) into Eq. (13) after lengthy but straightforward calculations, the medium PLDOS ρ_m is simplified as

$$\rho_m(\hat{\mathbf{r}}, \mathbf{r}_a, \omega) = \frac{3}{2} k_0^3 |\epsilon(\omega)|^2 \rho_0 \text{Im}[\epsilon(\omega)] (C_1(\mathbf{r}_a, \omega) + C_2(\mathbf{r}_a, \omega)), \quad (\text{A5})$$

where

$$C_1(\mathbf{r}_a, \omega) = \sum_n n^2 (n+1)^2 (2n+1) |A_N^{01}(\omega)|^2 \times \left| \frac{h_n^{(1)}(k_0 r_a)}{k_0 r_a} \right|^2 \int_0^a dr' r'^2 \left| \frac{j_n(k_1 r')}{k_1 r'} \right|^2, \quad (\text{A6a})$$

$$C_2(\mathbf{r}_a, \omega) = \sum_n n(n+1)(2n+1) |A_N^{01}(\omega)|^2 \times \left| \frac{h_n^{(1)}(k_0 r_a)}{k_0 r_a} \right|^2 \int_0^a dr' r'^2 |\partial_j j_n(k_1 r')|^2. \quad (\text{A6b})$$

Here, the following integral identities are used to get Eqs. (A6):

$$\int_0^\pi \frac{dP_n(\cos \theta')}{d\theta'} \frac{dP_{n'}(\cos \theta')}{d\theta'} \sin \theta' d\theta' = \frac{2n(n+1)}{2n+1} \delta_{nn'},$$

$$\int_0^\pi P_n(\cos \theta') P_{n'}(\cos \theta') \sin \theta' d\theta' = \frac{2}{2n+1} \delta_{nn'}.$$

APPENDIX B: SMALL-SPHERE APPROXIMATION

In the limit of a small sphere with $|k_1 a|, |k_0 a| \ll 1$ in which the wavelength of the atomic transition is large compared to the radius a of the sphere, the spherical Bessel and

Hankel functions appearing in Eqs. (A3) can be replaced by their Taylor expansions as $j_n(x) \simeq x^n/(2n+1)!!$ and $h_n^{(1)}(x) \simeq -i(2n-1)!!/x^{n+1}$ [82]. Using these Taylor expansions, we can also approximate the reflection and transmission coefficients in the small-sphere limit as

$$B_N^{00}(\omega) \approx \frac{i(n+1)(k_0 a)^{2n+1}}{(2n+1)!!(2n-1)!!} \left(\frac{\epsilon-1}{n\epsilon+n+1} \right), \quad (\text{B1a})$$

$$A_N^{01}(\omega) \approx \left(\frac{2n+1}{n\epsilon+n+1} \right) \left(\frac{k_0}{k_1} \right)^n. \quad (\text{B1b})$$

In what follows, we take into account two interesting cases where the atom is far from or very close to the sphere. For the short-distance limit where the atom is very close to the sphere the ratio a/r_a is very close to 1. In this case, the main contribution to the calculation of the PLDOS and the medium PLDOS comes from those terms corresponding to high orders of n . Therefore, the sum over n can be done by reducing it to some geometric sums [82]. Taking this into account and substituting Eq. (B1) into Eqs. (A4) and (A5), the PLDOS and the medium PLDOS read

$$\rho(\hat{\mathbf{r}}, \mathbf{r}_a, \omega) \simeq \rho_0 \left(1 + \frac{3}{8k_0^3} \text{Im} \left[\frac{\epsilon-1}{\epsilon+1} \right] z_a^{-3} \right), \quad (\text{B2a})$$

$$\rho_m(\hat{\mathbf{r}}, \mathbf{r}_a, \omega) \simeq \frac{3\rho_0}{4k_0^3} \text{Im}[\epsilon(\omega)] \left| \frac{1}{\epsilon+1} \right|^2 z_a^{-3}. \quad (\text{B2b})$$

While, in the long-distance limit where the condition $|k_0 r_a| \gg 1$ is satisfied, one finds that the leading-order term for calculating the PLDOS and the medium PLDOS for the small parameter a/r_a stems from the first spherical harmonic $n=1$ [83]. Keeping only this term and replacing (B1) and $h_1^{(1)}(k_0 r_a) \simeq -ie^{ik_0 r_a}/(k_0 r_a)^2$ in Eqs. (A4) and (A5), the PLDOS and the medium PLDOS are given by

$$\rho(\hat{\mathbf{r}}, \mathbf{r}_a, \omega) \approx \rho_0 \left(1 + \frac{6a^3}{k_0} \text{Im} \left[\frac{\epsilon-1}{\epsilon+2} \right] r_a^{-4} \right), \quad (\text{B3a})$$

$$\rho_m(\hat{\mathbf{r}}, \mathbf{r}_a, \omega) \approx \frac{18\rho_0}{k_0} \text{Im}[\epsilon(\omega)] \left| \frac{1}{\epsilon+2} \right|^2 r_a^{-4}. \quad (\text{B3b})$$

Note that the the small-sphere approximation is in exact agreement with the Markov approximation used here to get the master equation (4).

- [1] S. Pancharatnam, *Collected Works of S. Pancharatnam* (Oxford University Press, Oxford, 1975).
 [2] M. V. Berry, *Proc. R. Soc. London A* **392**, 45 (1984).
 [3] M. V. Berry, *Phys. Today* **43**(12), 34 (1990).
 [4] Y. Aharonov and D. Bohm, *Phys. Rev.* **115**, 485 (1959).
 [5] Y. Aharonov and J. Anandan, *Phys. Rev. Lett.* **58**, 1593 (1987).
 [6] J. Anandan and Y. Aharonov, *Phys. Rev. D* **38**, 1863 (1988).
 [7] J. Anandan, *Phys. Lett. A* **133**, 171 (1988).
 [8] J. Samuel and R. Bhandari, *Phys. Rev. Lett.* **60**, 2339 (1988).
 [9] A. K. Pati, *Phys. Rev. A* **52**, 2576 (1995).
 [10] F. Kleiβler, A. Lazariev, and S. Arroyo-Camejo, *npj Quantum Inf* **4**, 49 (2018).
 [11] Y.-Y. Huang, Y.-K. Wu, F. Wang, P.-Y. Hou, W.-B. Wang, W.-G. Zhang, W.-Q. Lian, Y.-Q. Liu, H.-Y. Wang, H.-Y. Zhang, L.

- He, X.-Y. Chang, Y. Xu, and L.-M. Duan, *Phys. Rev. Lett.* **122**, 010503 (2019).
 [12] Y.-W. Cho, Y. Kim, Y.-H. Choi, Y.-S. Kim, S.-W. Han, S.-Y. Lee, S. Moon, and Y.-H. Kim, *Nat. Phys.* **15**, 665 (2019).
 [13] M. T. Johnsson, N. R. Mukty, D. Burgarth, T. Volz, and G. K. Brennen, *Phys. Rev. Lett.* **125**, 190403 (2020).
 [14] T. Chen and Z.-Y. Xue, *Phys. Rev. Appl.* **14**, 064009 (2020).
 [15] J. Zhang, T. H. Kyaw, S. Filipp, L.-C. Kwek, E. Sjoqvist, and D. Tong, *Phys. Rep.* **1027**, 1 (2023).
 [16] R. K. L. Colmenar, U. Gungordu, and J. P. Kestner, *PRX Quantum* **3**, 030310 (2022).
 [17] R. S. Whitney and Y. Gefen, *Phys. Rev. Lett.* **90**, 190402 (2003).
 [18] R. S. Whitney, Y. Makhlin, A. Shnirman, and Y. Gefen, *Phys. Rev. Lett.* **94**, 070407 (2005).

- [19] A. Carollo, I. Fuentes-Guridi, M. F. Santos, and V. Vedral, *Phys. Rev. Lett.* **90**, 160402 (2003).
- [20] A. Carollo, *Mod. Phys. Lett. A* **20**, 1635 (2005).
- [21] D. M. Tong, E. Sjöqvist, L. C. Kwek, and C. H. Oh, *Phys. Rev. Lett.* **93**, 080405 (2004).
- [22] K. P. Marzlin, S. Ghose, and B. C. Sanders, *Phys. Rev. Lett.* **93**, 260402 (2004).
- [23] F. C. Lombardo and P. I. Villar, *Phys. Rev. A* **74**, 042311 (2006).
- [24] P. I. Villar and F. C. Lombardo, *Phys. Rev. A* **83**, 052121 (2011).
- [25] F. C. Lombardo and P. I. Villar, *Int. J. Quantum Inf.* **06**, 707 (2008).
- [26] F. C. Lombardo and P. I. Villar, *Phys. Rev. A* **81**, 022115 (2010).
- [27] F. C. Lombardo and P. I. Villar, *Phys. Rev. A* **87**, 032338 (2013).
- [28] P. I. Villar and A. Soba, *Phys. Rev. A* **101**, 052112 (2020).
- [29] J. Hu and H. Yu, *Phys. Rev. A* **85**, 032105 (2012).
- [30] J. J. Chen, J. H. An, Q. J. Tong, H. G. Luo, and C. H. Oh, *Phys. Rev. A* **81**, 022120 (2010).
- [31] G. De Chiara and G. M. Palma, *Phys. Rev. Lett.* **91**, 090404 (2003).
- [32] S. Banerjee and R. Srikanth, *Eur. Phys. J. D* **46**, 335 (2008).
- [33] X. X. Yi, L. C. Wang, and W. Wang, *Phys. Rev. A* **71**, 044101 (2005).
- [34] Z. S. Wang, C. Wu, X.-L. Feng, L. C. Kwek, C. H. Lai, and C. H. Oh, *Phys. Rev. A* **75**, 024102 (2007).
- [35] X. Cai, R. Meng, Y. Zhang, and L. Wang, *Europhys. Lett.* **125**, 30007 (2019).
- [36] L. Viotti, F. C. Lombardo, and P. I. Villar, *Phys. Rev. A* **105**, 022218 (2022).
- [37] I. Fuentes-Guridi, A. Carollo, S. Bose, and V. Vedral, *Phys. Rev. Lett.* **89**, 220404 (2002).
- [38] I. Fuentes-Guridi, S. Bose, and V. Vedral, *Phys. Rev. Lett.* **85**, 5018 (2000).
- [39] E. Martin-Martinez, I. Fuentes, and R. B. Mann, *Phys. Rev. Lett.* **107**, 131301 (2011).
- [40] M. B. Farias, F. C. Lombardo, A. Soba, P. I. Villar, and R. S. Decca, *npj Quantum Inf.* **6**, 25 (2020).
- [41] E. Martin-Martinez, A. Dragan, R. B. Mann, and I. Fuentes, *New J. Phys.* **15**, 053036 (2013).
- [42] B. Bellomo, R. Messina, and M. Antezza, *Europhys. Lett.* **100**, 20006 (2012).
- [43] B. Bellomo, R. Messina, D. Felbacq, and M. Antezza, *Phys. Rev. A* **87**, 012101 (2013).
- [44] X. Cai and Y. Zheng, *Phys. Rev. A* **94**, 042110 (2016).
- [45] J. M. Obrecht, R. J. Wild, M. Antezza, L. P. Pitaevskii, S. Stringari, and E. A. Cornell, *Phys. Rev. Lett.* **98**, 063201 (2007).
- [46] G. L. Klimchitskaya, U. Mohideen, and V. M. Mostepanenko, *Rev. Mod. Phys.* **81**, 1827 (2009).
- [47] P. W. Milonni, *The Quantum Vacuum* (Academic, San Diego, CA, 1994).
- [48] B. Huttner and S. M. Barnett, *Phys. Rev. A* **46**, 4306 (1992).
- [49] J. Jeffers, S. M. Barnett, R. Loudon, R. Matloob, and M. Artoni, *Opt. Commun.* **131**, 66 (1996).
- [50] L. G. Suttorp and M. Wubs, *Phys. Rev. A* **70**, 013816 (2004).
- [51] M. Amooshahi, *J. Math. Phys.* **50**, 062301 (2009).
- [52] F. Kheirandish, E. Amooghorban, and M. Soltani, *Phys. Rev. A* **83**, 032507 (2011).
- [53] T. G. Philbin, *New J. Phys.* **12**, 123008 (2010).
- [54] F. Kheirandish and E. Amooghorban, *Phys. Rev. A* **82**, 042901 (2010).
- [55] E. Amooghorban, M. Wubs, N. A. Mortensen, and F. Kheirandish, *Phys. Rev. A* **84**, 013806 (2011).
- [56] T. Gruner and D.-G. Welsch, *Phys. Rev. A* **53**, 1818 (1996).
- [57] H. T. Dung, L. Knöll, and D.-G. Welsch, *Phys. Rev. A* **57**, 3931 (1998).
- [58] S. Scheel, L. Knöll, and D.-G. Welsch, *Phys. Rev. A* **58**, 700 (1998).
- [59] R. Matloob, R. Loudon, S. M. Barnett, and J. Jeffers, *Phys. Rev. A* **52**, 4823 (1995).
- [60] L. Knöll, S. Scheel, and D.-G. Welsch, *Coherence and Statistics of Photons and Atoms* (Wiley, New York, 2001).
- [61] R. Matloob, *Phys. Rev. A* **70**, 022108 (2004).
- [62] M. Morshed Behbahani, E. Amooghorban, and A. Mahdifar, *Phys. Rev. A* **94**, 013854 (2016).
- [63] E. Amooghorban and E. Aleebrahim, *Phys. Rev. A* **96**, 012339 (2017).
- [64] P. Wu and H. Yu, *Phys. Rev. A* **92**, 062503 (2015).
- [65] H.-P. Breuer and F. Petruccione, *The Theory of Open Quantum Systems* (Oxford University Press, New York, 2002).
- [66] J. Hu, W. Zhou, and H. Yu, *Phys. Rev. D* **88**, 085035 (2013).
- [67] L. Novotny and B. Hecht, *Principles of Nano-Optics* (Cambridge University Press, Cambridge, England, 2006).
- [68] Z. Zhou, Y. Margalit, S. Moukouri, Y. Meir, and R. Folman, *Sci. Adv.* **6**, eaay8345 (2020).
- [69] P. J. Leek, J. M. Fink, A. Blais, R. Bianchetti, M. Göppl, J. M. Gambetta, D. I. Schuster, L. Frunzio, R. J. Schoelkopf, and A. Wallraff, *Science* **318**, 1889 (2007).
- [70] L. Viotti, F. C. Lombardo, and P. I. Villar, *Phys. Rev. A* **101**, 032337 (2020).
- [71] S. M. Abdhvand, E. Amooghorban, and A. Mahdifar, *IJPR* **20**, 235 (2020).
- [72] C. Kittel, *Quantum Theory of Solids* (Wiley, New York, 1987).
- [73] *Handbook of Optical Constants of Solids*, edited by E. Palik (Academic, New York, 1998).
- [74] E. A. Zibik, T. Grange, B. A. Carpenter, N. E. Porter, R. Ferreira, G. Bastard, D. Stehr, S. Winnerl, M. Helm, H. Y. Liu, M. S. Skolnick, and L. R. Wilson, *Nat. Mater.* **8**, 803 (2009).
- [75] D. I. Schuster, A. Wallraff, A. Blais, L. Frunzio, R.-S. Huang, J. Majer, S. M. Girvin, and R. J. Schoelkopf, *Phys. Rev. Lett.* **94**, 123602 (2005).
- [76] M. W. Doherty, N. B. Manson, P. Delaney, F. Jelezko, J. Wrachtrup, and L. C. L. Hollenberg, *Phys. Rep.* **528**, 1 (2013).
- [77] F. M. Cucchietti, J.-F. Zhang, F. C. Lombardo, P. I. Villar, and R. Laflamme, *Phys. Rev. Lett.* **105**, 240406 (2010).
- [78] S. Kollarics, B. G. Márkus, R. Kucsera, G. Thiering, Á. Gali, G. Németh, K. Kamarás, L. Forró, and F. Simon, *Sci. Adv.* **10**, eadn0616 (2024).
- [79] J. Jeske *et al.*, *Nat. Commun.* **8**, 14000 (2017).
- [80] A. D. Cronin, J. Schmiedmayer, and D. E. Pritchard, *Rev. Mod. Phys.* **81**, 1051 (2009).
- [81] L. W. Li, P. S. Kooi, M. S. Leong, and T. S. Yeo, *IEEE Trans. Microwave Theory Tech.* **42**, 2302 (1994).
- [82] S. Buhmann, *Springer Tracts in Modern Physics* (Springer, Berlin, 2013).
- [83] A. Sambale, S. Y. Buhmann, and S. Scheel, *Phys. Rev. A* **81**, 012509 (2010).